OXFORD

Cerebral Cortex, 2016, 1–10

doi: 10.1093/cercor/bhw125
Original Article

ORIGINAL ARTICLE

New Role of ATM in Controlling GABAergic Tone During Development

Lara Pizzamiglio[1,2], Elisa Focchi[2,3], Luca Murru[4], Matteo Tamborini[2], Maria Passafaro[4], Elisabetta Menna[3,4], Michela Matteoli[3,4] and Flavia Antonucci[2,4]

[1]Department of Biology and Biotechnology, Lazzaro Spallanzani, University of Pavia, 27100 Pavia, Italy, [2]Department of Biotechnology and Translational Medicine, University of Milan, 20129 Milan, Italy, [3]Humanitas Clinical and Research Center, IRCCS Rozzano, Rozzano (Milan), Italy and [4]Institute of Neuroscience, C.N.R., 20129 Milan, Italy

Address correspondence to Flavia Antonucci. Email: f.antonucci@in.cnr.it or flavia.antonucci@unimi.it

Elisa Focchi and Luca Murru shared second authors.

Abstract

The capacity to guarantee the proper excitatory/inhibitory balance is one of the most critical steps during early development responsible for the correct brain organization, function, and plasticity. GABAergic neurons guide this process leading to the right structural organization, brain circuitry, and neuronal firing. Here, we identified the ataxia telangiectasia mutated (ATM), a serine/threonine protein kinase linked to DNA damage response, as crucial in regulating neurotransmission. We found that reduced levels of ATM in the hippocampal neuronal cultures produce an excitatory/inhibitory unbalance toward inhibition as indicated by the higher frequency of miniature inhibitory postsynaptic current events and an increased number of GABAergic synapses. In vivo, the increased inhibition still persists and, even if a higher excitation is also present, a reduced neuronal excitability is found as indicated by the lower action potential frequency generated in response to high-current intensity stimuli. Finally, we found an elevated extracellular signal-regulated kinase 1/2 (ERK1/2) phosphorylation in heterozygous hippocampi associated with lower expression levels of the ERK1/2 phosphatase PP1. Given that the neurodegenerative condition associated with genetic mutations in the *Atm* gene, ataxia telangiectasia, presents a variable phenotype with impairment in cognition, our molecular findings provide a logical frame for a more clear comprehension of cognitive defects in the pathology, opening to novel therapeutic strategies.

Key words: ATM, hippocampus, KCC2, kinase–phosphatase cycle

Introduction

The maintenance of the balance between excitation and inhibition is one of the most critical steps during early development necessary to guarantee correct brain functions and properties such as circuitry formation (Hensch and Fagiolini 2005; Gogolla et al. 2009; Nakayama et al. 2012; Succol et al. 2012), activity-dependent tuning of neuronal networks, and neuronal plasticity (Harauzov et al. 2010; Sale et al. 2010; Maya-Vetencourt et al. 2012; Deidda et al. 2015). In particular, GABAergic expansion, preceding the glutamatergic input–output building (Khazipov et al. 2001), instructs neurons for all these purposes and for a fine brain functioning.

Ataxia telangiectasia mutated (ATM) is a serine/threonine protein kinase whose function has been principally associated

with DNA damage response. Upon recruitment and activation by DNA double-strand breaks, it phosphorylates several key proteins, mostly tumor suppressors such as p53, CHK2, and H2AX, that initiate activation of the DNA damage checkpoint, leading to cell cycle arrest, DNA repair, and apoptosis (Khanna and Jackson 2001; Aloj et al. 2012). Even if ATM roles during cell division have been largely addressed, a large body of evidence clearly demonstrated new functions of ATM also in adult neurons, suggesting the lack of a complete understanding of ATM functions. As an example, $ATM^{+/-}$ and $ATM^{-/-}$ cells are still capable of guaranteeing DNA repair mechanisms even if through more time-consuming pathways (Herrup et al. 2013). In addition, many abnormalities have been described in $ATM^{-/-}$ neuronal stem cells (Allen et al. 2001), including defective proliferation and differentiation along the neuronal lineage, thus suggesting that ATM plays a role in adult neurogenesis. Also, a number of observations indicate that ATM-deficient cells are hypersensitive to oxidative stress-inducing agents (hydrogen peroxide) and that radical scavengers can alleviate this sensitivity (Lee et al. 2006). Finally, some studies demonstrated a possible role of ATM at the synapse formed by cerebellar granule cells, as suggested by its interaction with β-adaptin in synaptic vesicles (Lim et al. 1998). Finally, ATM kinase has been found to form a complex with 2 synaptic vesicle proteins, VAMP2 and synapsin I, indicating a possible contribution of ATM in the synaptic vesicles release at cortical synapses (Li et al. 2009) and suggesting that the absence of the protein can be responsible for the generation of neuronal dysfunctions.

Consistently, the neurodegenerative condition associated with genetic mutations in the *Atm* (A-T mutated) gene, the ataxia telangiectasia (A-T), displays besides cerebellar atrophy, immune dysfunctions (Chun and Gatti 2004), genomic instability, predisposition to cancer (Chun and Gatti 2004; Aloj et al. 2012), and cognitive impairments, such as speech defects and abnormalities, in late learning that do not originate exclusively from cerebellum. In fact, by using positron emission tomography, a reduced neuronal metabolism has been described not only in the cerebellum but also in the hippocampus (as well as in other deep brain structures) in heterozygous A-T patients (Volkow et al. 2014). Thus, ATM may impact brain functions through distinct mechanisms both in different brain regions and in diverse cell populations. To directly address these new and unclear aspects of ATM in adult neurons and supported by the observations that cognitive noncerebellar defects occur in milder form of A-T with residual ATM kinase activity (Borghesani et al. 2000), we investigated whether and at which extent reduction in ATM levels impacts hippocampal function. We found that 50% levels of ATM in hippocampal neuronal cultures produce an excitatory/inhibitory unbalance toward inhibition as indicated by the higher frequency of inhibitory postsynaptic current (IPSC) miniature events, the increased number of GABAergic inhibitory synapses, and a more precocious development of the inhibitory system (i.e., excitatory to inhibitory GABA switch) as observed in both chronic and acute reduction of the protein. These rearrangements seem to result from a process involving the extracellular signal-regulated kinase 1/2 (P-ERK 1/2), protein phosphatase 1 (PP1) phosphatase, and the calcium-dependent protease calpain. In vivo, we found the development of a more complex phenotype characterized by lower excitability, despite the occurrence of both higher GABAergic and glutamatergic neurotransmission. These data identify novel functions of ATM in neurons and lay the basics for a more clear comprehension of cognitive defects occurring in A-T.

Results

Enhanced Inhibitory Transmission in $ATM^{+/-}$ Hippocampal Cultured Neurons

We stained hippocampal cultured neurons with specific antibodies against ATM, the neuronal marker NeuN, and the inhibitory neurons (anti-GAD) to evaluate the possible preferential localization/expression of ATM in post-mitotic cells. As indicated in Supplementary Figure 1, we found a ubiquitously localization of ATM in the adult neuronal populations as well as in astrocytes. To evaluate electrophysiological features of neurons with reduced ATM protein levels, we prepared hippocampal cultures from $ATM^{+/+}$ and $ATM^{+/-}$ embryos, which express 50% of the protein levels in the hippocampus (see Supplementary Fig. 1B). Glutamatergic and GABAergic miniature excitatory and inhibitory postsynaptic currents (mEPSCs and mIPSCs) were recorded by patch-clamp in the presence of 1 μM tetrodotoxin (TTX) from 13 to 15 days in vitro (DIV) cultured hippocampal neurons established from $ATM^{+/+}$ and $ATM^{+/-}$ embryos (Fig. 1A). Whereas no significant differences in mEPSC frequency (freq) were detected [freq: wild type (wt) = 2.8 ± 0.2 Hz (20 neurons) vs. heterozygous (het) = 2.3 ± 0.1 Hz (29 neurons); *t*-test: $P = 0.1$; Fig. 1B; number of coverslips = 5 for group], increased frequency of mIPSCs was recorded from $ATM^{+/-}$ (het) neurons with respect to the wt [freq: wt = 1.0 ± 0.1 Hz (21 neurons) vs. het = 1.46 ± 0.09 Hz (27 neurons); *t*-test: $P = 0.013$; Fig. 1B; number of coverslips = 4 for group], thus indicating the possible occurrence of an unbalance between excitation and inhibition in het hippocampal cells. A detailed analysis of mIPSCs from $ATM^{+/-}$ neurons showed the lack of differences in amplitude, decay time, and quantal charge (see Supplementary Fig. 1C), suggesting selective alterations mediated by the ATM loss at the presynaptic level. Measurement of inhibition/excitation (I/E) ratio analyzed in individual cells confirmed an enhanced inhibitory tone in hippocampal $ATM^{+/-}$ neurons with respect to their wt counterpart (wt = 0.42 ± 0.07 vs. het = 0.77 ± 0.08; *t*-test: $P = 0.001$; Fig. 1C). Furthermore, hypertonic sucrose solution (Fig. 1D) delivery indicated an increased charge transferred at the inhibitory synapse (Fig. 1Ea). This would be consistent with a higher number of inhibitory vesicles released at the heterozygous hippocampal synapses with respect to their wt counterpart (normalized number of vesicles, wt = 1.0 ± 0.2 vs. het = 2.2 ± 0.3; *t*-test: $P = 0.038$; Fig. 1Eb), without, however, excluding increased probability of release. Chronic delivery (from DIV 6 to 11) of low doses of the GABA receptor inhibitor, bicuculline (5 μM), did not produce changes in synaptic vesicle accumulation in wt neurons [Fig. 1Ec,d, wt = 1.0 ± 0.1 ($n = 10$) vs. wt post-bicuculline = 0.9 ± 0.2 ($n = 11$); *t*-test: 0.59], but was effective in rescuing the higher number of inhibitory vesicles as evaluated in het cultures [Fig. 1Ec,d, het = 1.0 ± 0.2 ($n = 8$) vs. het post-bicuculline = 0.5 ± 0.1 ($n = 9$), *t*-test: $P = 0.046$; normalized value with respect to the het number of vesicles]. Conversely, the increment in mIPSC frequency found in heterozygous neurons with respect to wt remained unmodified after bicuculline treatment [mIPSC frequency (Hz)—data not shown: wt = 1.0 ± 0.1 vs. wt post-bicuculline = 1.0 ± 0.2; *t*-test: 0.65; het = 1.3 ± 0.3 Hz vs. het post-bicuculline = 1.6 ± 0.2 Hz, *t*-test: $P = 0.43$], suggesting the coincidence of multiple mechanisms associated with ATM deficiency. In addition, immunocytochemical experiments in 15 DIV het cultured neurons showed a higher mean fluorescence intensity of synaptic puncta positive for the vesicular GABA transporter vGAT occurring in the absence of changes in the vesicular glutamate transporter vGLUT-positive puncta (Fig. 1F, vGlut: wt = 192.7 ± 2.7 vs. het = 194.1 ± 0.5, *t*-test: $P > 0.05$; vGAT:

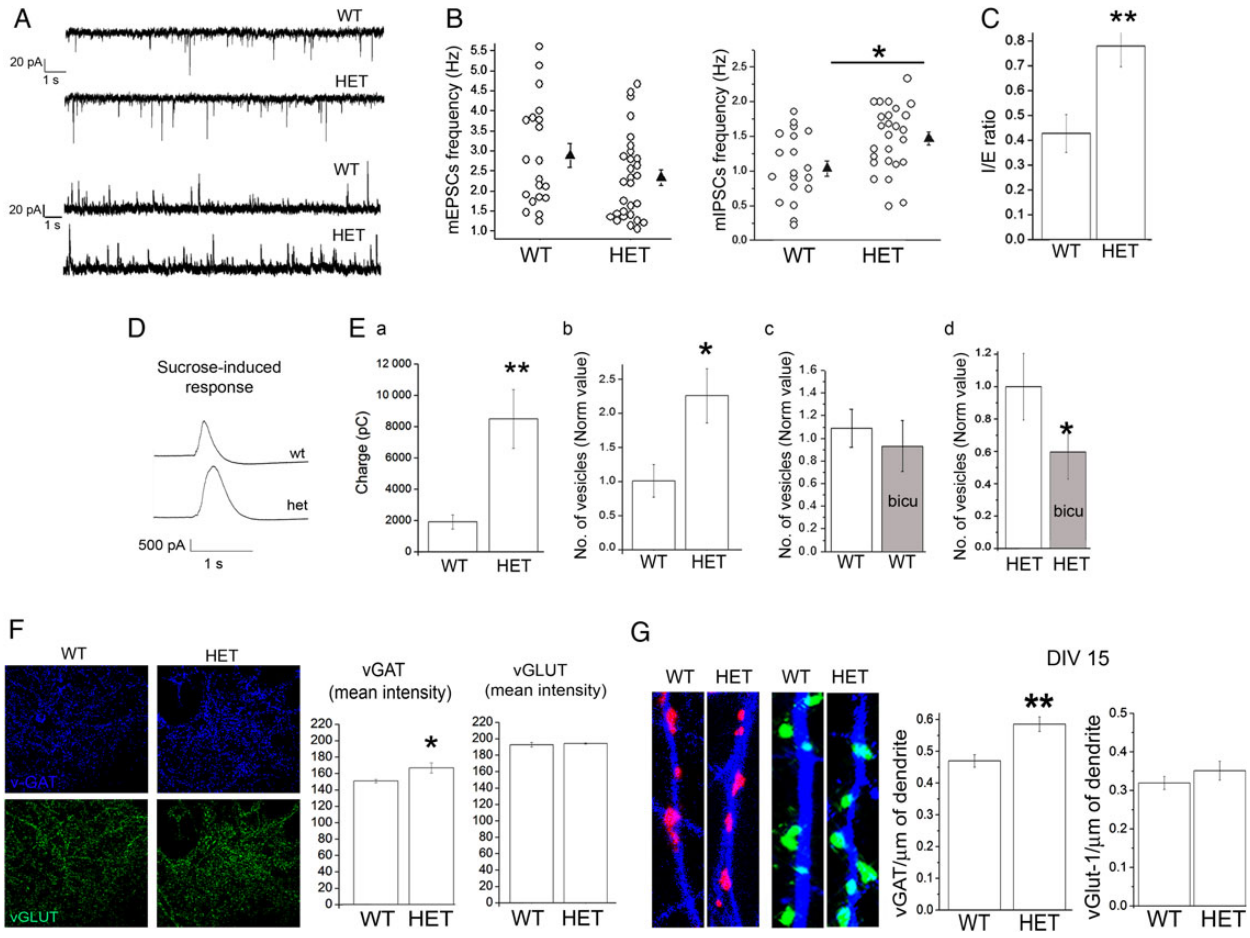

Figure 1. (*A*) Representative traces of mIPSCs and mEPSCs recorded in DIV 13–14 mouse cultured neurons obtained from $ATM^{+/+}$ and $ATM^{+/-}$ embryos. (*B*) Analysis of excitatory and inhibitory frequency from cultured neurons. (*C*) I/E ratio from het and wt cultured neurons clearly indicates the predominance of inhibitory events. (*D*) Representative inhibitory responses after sucrose stimulation in DIV 15 cultures. (*Ea–d*) Evaluation of charge transferred by hypertonic sucrose experiments (a) and quantification of inhibitory synaptic vesicle in het neurons versus wt (b) or in wt (c) and het (d) neurons post-bicuculline treatment. (*F*) Left: immunocytochemical images of neurons labeled against α-vGAT and α-vGlut-1 antibody. Right: analysis of α-vGAT and α-vGlut intensity fluorescence from $ATM^{+/+}$ (WT) and $ATM^{+/-}$ (HET) neurons. (*G*) Immunocytochemical experiments performed in wt and het cultured neurons showing (left) vGAT-positive puncta (red) per unit length of dendrite (blue; β–tubulin-positive filament) and corresponding quantitative analysis or vGlut-1-positive puncta (green) per unit length of dendrite.

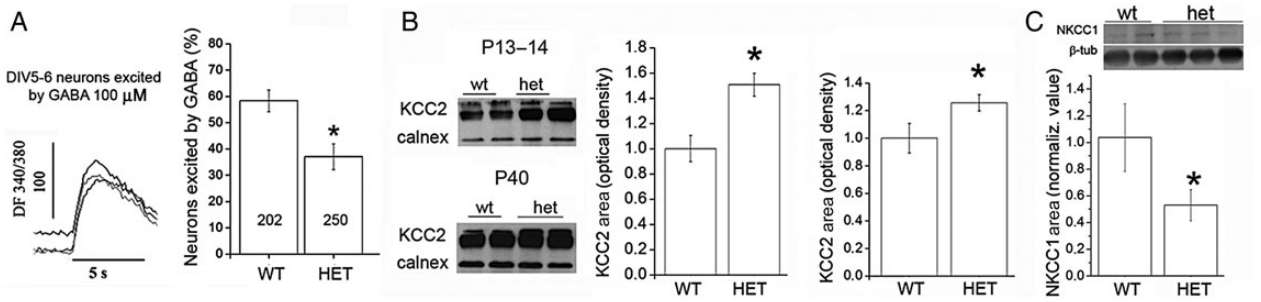

Figure 2. (*A*) Calcium imaging responses to acute GABA administration (100 µM) in DIV 6 cultured hippocampal neuron from wt and het embryos and percentage of responding neurons (202 versus 250 cells) analyzed from wt and het cultured neurons; note that the different gray-scale lines indicate 3 distinctive representative calcium transients in wt neurons responding to GABA stimulus. (*B*) Western blotting and analyzed data of P14 and P40 hippocampal tissues showing the augmented KCC2 signal. (*C*) Evaluation of NKK1 signal in P14 animals.

wt = 148.7 ± 2 vs. het = 164.5 ± 5.9; *t*-test: $P = 0.022$). In parallel, we observed an increased number of vGAT-positive puncta per unit length of isolated parent dendrite chosen by positive tubulin immunoreactivity (Fig. 1*G*, wt = 3 coverslips prepared from 3 different embryos vs. het = 4 coverslips prepared from 4 different embryos; number of vGAT-positive puncta/µm: wt = 0.46 ± 0.01 vs. het = 0.58 ± 0.02; *t*-test: $P = 0.005$), thus suggesting that ATM deficiency leads to increased density of inhibitory synapses. The same analysis performed at excitatory synapses did not show any difference in the density of vGlut-positive puncta per µm of parent dendrites from wt and het neurons, supporting the hypothesis of an unbalance between the GABAergic and

Glutamatergic functional synapses in cultured neurons expressing half ATM kinase (Fig. 1G, wt = 3 coverslips prepared from 3 different embryos vs. het = 4 coverslips prepared from 4 different embryos; number of vGlut-1-positive puncta/µm: wt = 0.32 ± 0.01 vs. het = 0.35 ± 0.02, *t*-test: $P = 0.23$).

Altered GABA Switch in $ATM^{+/-}$ Neuronal Networks

We then investigated whether the development of GABAergic inhibitory function was accelerated in $ATM^{+/-}$ neurons by investigating the so-called GABA switch in hippocampal het cells. Single cell Ca^{2+} imaging was then employed to monitor GABA-evoked Ca^{2+} influx to determine whether GABA action is excitatory or inhibitory (van den Pol et al. 1996). It is described that at 5–6 DIV, about 60% of neurons still respond to GABA (100 µM) with calcium transients (i.e., GABA depolarizing action; Sun et al. 2013). Whereas these data were fully confirmed in wt cultures (wt responding = 58.2 ± 4%), only 37 ± 4% of $ATM^{+/-}$ neurons responded to GABA with calcium transients (*t*-test: $P = 0.014$; Fig. 2A; number of coverslips: wt = 8 vs. het = 9 corresponding to 8 and 9 different embryos). These data indicate a precocious GABA switch associated with *ATM* heterozygosity. Since KCC2 is responsible for GABA switch (Lu et al. 1999), we investigated the KCC2 immunoreaction by western blotting experiments. KCC2 is the neuron-specific K^+–Cl^- co-transporter that constitutes the main extruder of Cl^- in mature neurons (Rivera et al. 1999). It is expressed at low levels in immature cells, causing cell depolarization upon GABA stimulation (Ben-Ari et al. 1989; Cherubini et al. 1991) and its increment during development is associated with the final hyperpolarizing effects of GABA (GABA switch; Lu et al. 1999). To evaluate the possible occurrence of alterations in KCC2 levels, we looked at the KCC2 signal in the hippocampal tissues by western blotting in the 2 different developmental aged mice P13 and P40. As shown in Figure 2B, we found a higher KCC2 expression in the het phenotype with respect to the wt one, thus supporting the hypothesis that half ATM results in a more precocious GABAergic development mediated by higher KCC2 levels [Chudotvorova et al. 2005; normalized value, P13—Fig. 2B, left: wt = 0.98 ± 0.05 ($n = 5$) vs. het = 1.50 ± 0.09 ($n = 9$), *t*-test: $P = 0.034$; P40—Fig. 2B, right: wt = 1.0 ± 0.1 ($n = 3$) vs. het = 1.25 ± 0.05 ($n = 9$), *t*-test: $P = 0.027$]. Also, western blotting experiments performed on only male P13 mice revealed the same differences in the KCC2 expression [normalized value, P13—wt = 1 ($n = 3$) vs. het = 1.3 ± 0.1 ($n = 4$)]. Since KCC2 expression is inversely associated with NKCC1 expression, we also evaluated NKCC1 expression and found a reduction of NKCC1 signal in P13 het hippocampi with respect to the wt [Fig. 2C; wt = 1.0 ± 0.2 ($n = 4$) vs. het = 0.5 ± 0.1 ($n = 9$), *t*-test: $P = 0.034$]. NKCC1 was undetectable in our P40 hippocampal tissues from both het and wt samples, in accordance with the downregulation of protein expression during the brain development.

Higher ERK1/2 Phosphorylation and Reduced PP1 Phosphatase expression

Since previous studies revealed a clear link between phosphorylation of ERK1/2 and KCC2 expression through the rapid Egr4-dependent activation of the KCC2b promoter (Ludwig et al. 2011), we quantified the levels of phosphorylated ERK1/2 (active ERK1/2) in the hippocampi of P13 and P40 $ATM^{+/-}$ mice. We found a significant increase in the levels of phosphorylated ERK1/2 in P13 and P40 $ATM^{+/-}$ hippocampi [P13: wt = 1.0 ± 0.1 ($n = 6$) vs. het = 1.7 ± 0.2 ($n = 15$), *t*-test: $P = 0.011$; P40: wt = 0.9 ± 0.2 ($n = 3$) vs. het = 4.5 ± 0.7 ($n = 5$), *t*-test = 0.001; Fig. 3A,B]. In P40 mice (where the strongest ERK phosphorylation was detected), the higher ERK1/2 phosphorylation was not associated with higher levels of total ERK1/2 [Fig. 3B, wt = 1.00 ± 0.01 ($n = 2$) vs. het = 1.1 ± 0.1 ($n = 4$)], thus demonstrating that reduced ATM is associated specifically with a pronounced increment of ERK1/2 phosphorylation. To define the molecular mechanisms underlying the enhanced ERK1/2 phosphorylation in $ATM^{+/-}$ hippocampi, we focused on the protein phosphatases acting on P-ERK1/2, calcineurin A, and the PP1. Western blotting analysis revealed no significant differences in calcineurin A levels in $ATM^{+/-}$ hippocampi between both experimental groups (see Supplementary Fig. 2), indicating that the higher levels of phospho-ERK in $ATM^{+/-}$ mice could not be secondary to alterations of calcineurin A levels.

Conversely, PP1 levels were found significantly lower in both P13 and P40 $ATM^{+/-}$ hippocampi [P13: wt = 1.0 ± 0.2 ($n = 6$) vs.

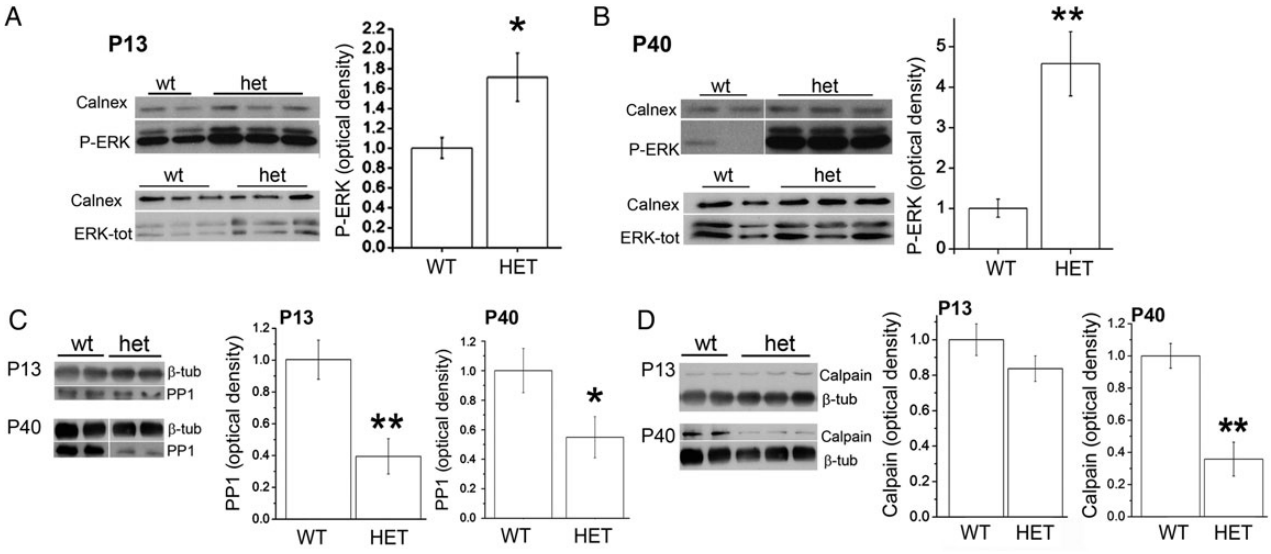

Figure 3. (*A* and *B*) Biochemical experiments carried out in P13 and P40 wt and het mice showing the higher phosphorylation of ERK 1/2 in ATM-depleted hippocampi with respect to the total ERK expression. (*C* and *D*) PP1 and calpain signals revealed by western blotting in young and adult tissues and corresponding quantification.

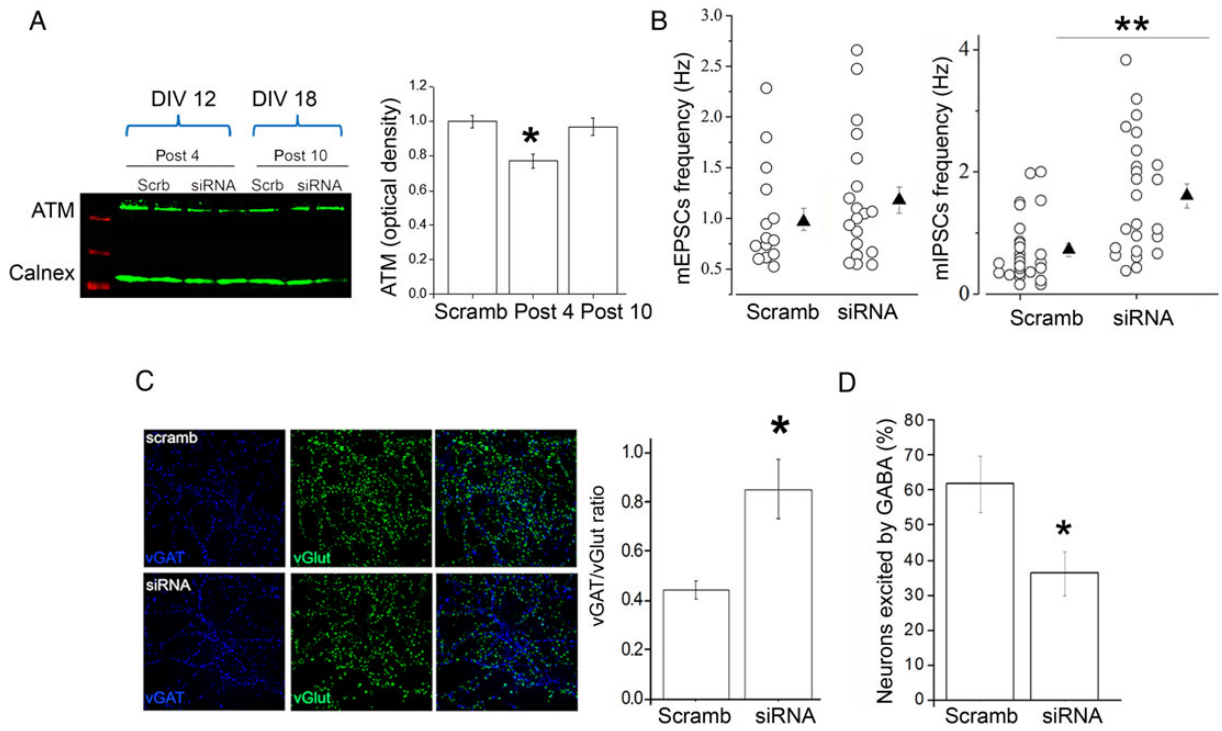

Figure 4. (*A*) Evaluation of acute downregulation of ATM expression by specific siRNA with biochemistry; 10 days after the siRNA treatment, the ATM signal was found comparable with respect to the scrambled one. (*B*) Analyses of mEPSC and mIPSC frequency have been evaluated in DIV 12–13 hippocampal rat neurons 4–5 days after siRNA delivery. (*C*) Immunocytochemical experiments carried out in siRNA-treated neurons to evaluate vGAT/vGlut ratio. (*D*) Calcium imaging responses to acute GABA administration (100 μM) in DIV 7 cultured rat hippocampal neuron transfected at DIV 2 and quantification of the responding neurons.

het = 0.3 ± 0.1 (n = 9), t-test: P = 0.015; P40: wt = 1.0 ± 0.1 (n = 6) vs. het = 0.5 ± 0.1 (n = 7), t-test: P = 0.040; Fig. 3*C*], suggesting that higher P-ERK levels could be associated with lower levels of PP1 phosphatase. This could be possibly due to a positive interaction between ATM and PP1, making PP1 more unstable in the absence of ATM. In line with this finding, a recent report demonstrated a direct ATM-dependent activation of PP1 (Guo et al. 2007), thus supporting this possible mechanism in the $ATM^{+/-}$ mouse model.

Furthermore, given that KCC2 has been identified as a new target of calpain (Chamma et al. 2013; Shiloh 2006) and since calpain seems to display a higher proteolytic activity in GABAergic neurons (Grumelli et al. 2008), we analyzed calpain levels in $ATM^{+/-}$ hippocampi by western blotting. Although calpain levels resulted highly variable in tissues explanted from P13 wt mice, a significant reduction in P40 $ATM^{+/-}$ hippocampi was detected [P13: wt = 1.0 ± 0.1 (n = 4) vs. het = 0.7 ± 0.1 (n = 9), t-test: P = 0.3; P40: wt = 1.00 ± 0.07 (n = 7) vs. het = 0.3 ± 0.1 (n = 9); t-test = 0.004; Fig. 3*D*], suggesting that this mechanism could contribute to the altered levels of KCC2 in $ATM^{+/-}$ mice. Altogether, these results indicate that halved levels of ATM are associated with enhanced ERK activation, and point out that reduced levels of PP1 and calpain may be at the origin of this process. These alterations may eventually impact the Egr4 transcription factor activation.

Acute Downregulation of ATM by Specific siRNA Produces the Same Functional Modifications Occurring in Constitutively ATM-Depleted Neurons

To directly link changes in ATM expression with alterations in the GABAergic neurotransmission and to exclude the involvement of functional/anatomical rearrangements in *ATM* het neurons during development, acute protein downregulation by siRNAs was carried out in rat cultured hippocampal neurons and electrophysiological recordings were performed. Eight DIV neurons were transfected and examined 3–4 days later. Around 20–30% reduction in ATM signal was measured by western blotting experiments (Fig. 4*A*), thus ensuring a good amount of residual ATM. Analysis of mIPSCs and mEPSCs revealed alterations in excitatory/inhibitory unbalance similar to those already detected in het neurons. Indeed, enhanced mIPSC, but not mEPSC, frequency (Fig. 4*B*, scramb = 0.7 ± 0.1 Hz; siRNA = 1.6 ± 0.1 Hz; t-test: $P < 0.001$; n = 26 vs. 24 neurons patched) was detected in siRNA-treated cells, whereas no difference was observed in mIPSC amplitude (scramb = 1.0 ± 0.1 Hz; siRNA = 1.1 ± 0.1 Hz; t-test: $P > 0.05$; amplitude: scramb = 15.1 ± 0.6 pA vs. siRNA = 17.2 ± 1.1 pA, t-test: $P > 0.05$). Furthermore, immunocytochemical experiments carried out to evaluate vGAT/vGlut ratio in siRNA-treated neurons revealed the occurrence of a shift in favor of vGAT-immunopositive synaptic puncta in ATM-depleted neurons with respect to scrambled-treated controls (Fig. 4*C*, scramb = 0.44 ± 0.03 vs. siRNA = 0.8 ± 0.1; t-test: P = 0.03; n = 2 coverslips analyzed for each group). Finally, reduction of ATM at earlier developmental stages produced the same anticipated GABAergic functional development as revealed by Ca^{2+} imaging experiments conducted on DIV 6 neurons transfected at DIV 2 (Fig. 4*D*, % of responding neurons: scramb = 61.3 ± 5.4; siRNA = 42.2 ± 5.4; t-test: P = 0.017, number of total neurons scramb = 100, siRNA = 155, from 3 different coverslips/group). Altogether, these data indicate that also acute reduction of ATM impacts on the normal neuronal development by producing a potentiated/anticipated GABAergic tone.

Functional Changes in $ATM^{+/-}$ Mouse Hippocampus

Finally, in order to investigate whether and at which extent the unbalanced neurotransmission found in cultures is detectable also in vivo, we recorded hippocampal activity in slices from

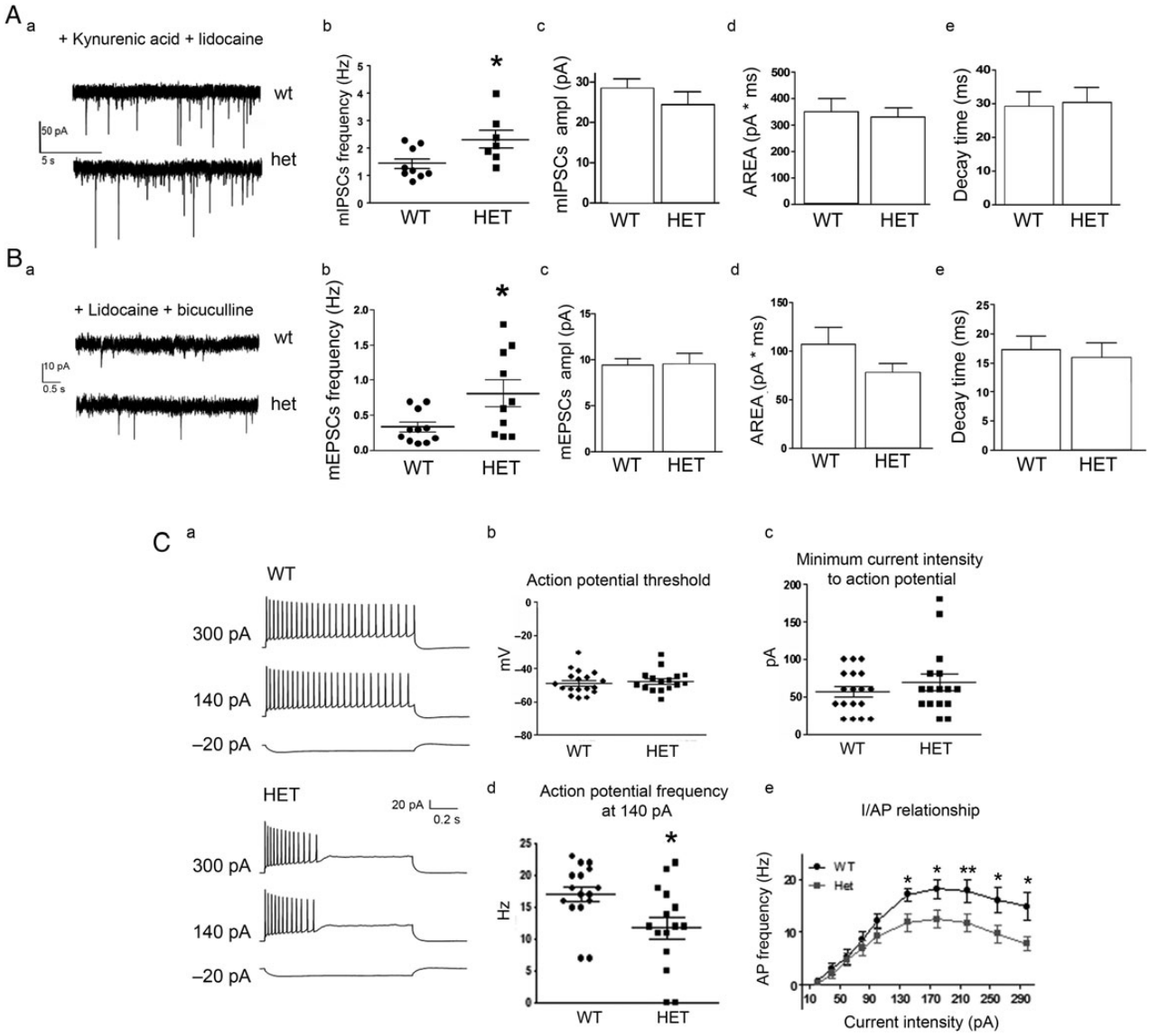

Figure 5. (A) (a) Electrophysiology of hippocampal brain slices showing mIPSCs and corresponding quantification of frequency in Hz (b). Note that amplitude (c), quantal charge (d), and decay time (e) remain unchanged in the 2 groups as well as what found in het cultured cells. (Ba–e) Representative traces and corresponding quantification of in vivo slice electrophysiology assessed to evaluate excitatory basal transmission (mEPSCs) as done for mIPSCs. (C) (a) Analysis of pyramidal intrinsic excitability properties by whole-cell current-clamp recordings from hippocampal slices in P40 male mice. (b–e) Evaluation of AP threshold, MCI to generate an action potential and increasing current stimuli with associated frequency response. All these recordings have been carried out from hippocampal slices of male P40 WT and HET animals.

postnatal day 40 (P40) wt and $ATM^{+/-}$ mice. Analysis of passive membrane properties in CA1 pyramidal neurons such as resting membrane potential, capacitance, input resistance, and I/V relationship indicated the lack of differences between the 2 experimental groups (see Supplementary Fig. 3). In line with these data collected in cultured neurons, a significant increase in mIPSC frequency (wt = 1.4 ± 0.1 Hz vs. het = 2.3 ± 0.3 Hz, t-test: $P = 0.029$; Fig. 5Aa,b) was found in *ATM* het mice. However, analysis of excitatory miniature activity from hippocampal slices revealed a concomitant higher frequency of glutamatergic events (Fig. 5Ba,b, mEPSCs: wt = 0.33 ± 0.06 Hz vs. het = 0.8 ± 0.1 Hz, t-test: $P = 0.022$) in the absence of changes in the amplitude, minis area, and decay time of both inhibitory and excitatory minis (Fig. 5Ac–e,Bc–e). Thus, in order to assess how the reduction of ATM could impact active neuronal properties, we assessed the intrinsic excitability in wt and het neurons by whole-cell current-clamp recordings from P40 mice (Fig. 5Ca). When depolarizing current stimuli were applied to evaluate action potential (AP) firing properties, a comparable behavior in terms of AP threshold and minimum current intensity (MCI) to generate an AP was found between het and wt neurons as indicated in Figure 5Cb,c (AP threshold: wt = –48.6 ± 1.6 mV vs. het = –47.6 ± 1.6 mV; t-test: $P = 0.64$; MCI to AP: wt = 56.6 ± 6.7 pA vs. het = 68.7 ± 1.2 pA; t-test: $P = 0.35$). Interestingly, a reduction in firing frequency/current injection relationship was found in $ATM^{+/-}$ slices as indicated by the lower mean number of spikes fired for each current amplitude with increased current injection (AP frequency at 140 pA: wt = 17.1 ± 1.1 Hz vs. het = 11.9 ± 1.7 Hz; t-test: $P = 0.015$; Fig. 5Cd, e). Altogether, these results indicate that hippocampal pyramidal neurons from heterozygous animals are less excitable than wt

counterparts even in the presence of comparable passive properties.

Finally, to complete the in vivo characterization of $ATM^{+/-}$ hippocampal features, we analyzed the expression of inhibitory synaptic proteins such as vGAT during the hippocampal development. vGAT western blotting signal collected from P14 and P40 mouse hippocampus revealed comparable levels of the protein at both ages [see Supplementary Fig. 4A, P14 normalized value: wt = 1.00 ± 0.05 (n = 7) vs. het = 1.2 ± 0.1 (n = 9); P40 mice: wt = 1.00 ± 0.04 (n = 8) vs. het = 1.2 ± 0.1 (n = 9)]. Analysis of vGAT signal in the cerebellum and P40 and P120 het mice showed no differences with respect to the corresponding wt littermates (see Supplementary Fig. 4B). Interestingly, evaluation of vGAT expression in the cerebellum at earlier developmental stages (P13) revealed higher levels of the inhibitory marker in het tissues with respect to the wt counterpart (see Supplementary Fig. 4C), indicating a transient vGAT upregulation in developing cerebellum of *ATM* het mice. Thus, these data indicate the occurrence of pathological changes in the inhibitory system during the early phases of development, which may sustain altered network activity in adult. Therefore, halved levels of ATM, by affecting the brain inhibitory component during development, impact hippocampal functioning both in vitro and in vivo.

Discussion

In this study, we demonstrate that alterations in ATM levels are responsible for pronounced and anticipated GABAergic development and function. Since GABA transmission is strongly linked to the correct brain development and plasticity, this study lays basics for both a more clear comprehension of mechanisms associated with brain development and of molecular alterations possibly involved in cognitive alterations described in A-T. This study provides a rationale for the defects described in the milder forms of A-T characterized by residual amounts of functional ATM and associated with later onset, slower progression of symptoms, and by cognitive defects such as late learning and altered speech proprieties, introducing a novel potential target for emerging therapeutic approaches. This study supports previous evidence that the pleiotropic phenotype found in A-T patients may be ascribed in part to tissue- and age-specific regulation of diverse pathways in vivo. Indeed, by exploring the fully uninvestigated hippocampal role of ATM during brain development using the heterozygous mouse model of A-T, we show the occurrence of a clear changing in the neuronal networks developing in the presence of chronic and acute reduced levels of ATM. This alteration, which has been clearly revealed by electrophysiological and biochemical experiments, is consistent with studies highlighting inhibition as a pathological rearrangement responsible, in general, for impaired neuronal development (Tyzio et al. 2006, 2014; Gogolla et al. 2009) or altered circuitry formation (Di Cristo 2007; Antonucci et al. 2012) and abnormal neuronal plasticity (Hensch 2005; Di Cristo 2007; Harauzov et al. 2010; Sale et al. 2010; Maya-Vetencourt et al. 2012; Succol et al. 2012; Deidda et al. 2015). In particular, whereas a clear excitatory/inhibitory unbalance develops in hippocampal neuronal cultures, a more complex phenotype is generated in vivo. Although in the presence of both higher mEPSCs and mIPSCs, adult heterozygous animals show reduced excitability, as indicated by the reduced AP frequency generated in response to high-current intensity stimuli. We hypothesize that this decreased neuronal excitability could result from possible compensatory mechanisms likely stemming from enhanced activity of the GABAergic transmission or by the higher K^+ current flowing through KCC2, which we found to be expressed at higher levels in het animals. Finally, it has been also described that an overall enhancement of GABAergic transmission, in the presence of a higher miniature excitatory activity, can still sustain a reduction in intrinsic excitability (He et al. 2010). On the other hand, the neurotransmitter GABA acting as a trophic factor in many aspects of neural development, including cell proliferation, neuronal migration, dendrite arborization, synapse formation, and activity-dependent neural circuit development (Ben-Ari 2002; Owens and Kriegstein 2002; Akerman and Cline 2007), can also mediate the increment in excitatory synaptic transmission that we found by whole-cell recordings in slice. In this context, it could be also interesting to evaluate if this more pronounced GABAergic inhibition leads to altered neuronal response induced by excitatory/convulsant stimuli, in vivo (i.e., the kainic acid-induced excitability). However, further studies are needed to better clarify cellular mechanisms associated with the increased excitatory events found by in vivo analysis of mEPSCs.

In addition, our results demonstrate that the enhanced inhibition is present not only in the hippocampus but also at early stages of cerebellar development, thus extending the main data found in the hippocampus to other brain structures. The mechanism we propose here concerns the unbalance of phosphorylation/dephosphorylation processes involving protein kinases and phosphatase. In a previous study, decreased Ca^{++} and Na^+ currents were detected by electrophysiological experiments on Purkinje cells in the A-T mouse model, which was not associated with any neuronal loss and neurodegeneration (Chiesa et al. 2000). To explain their results, the authors proposed the involvement of ATM in the phosphorylation/phosphatase cycle acting on Ca^{++} channels. Indeed, since the "function of Ca^{++} channels is greatly dependent on their state of phosphorylation, it is possible that the lack of ATM leads to an imbalance of phosphorylation processes involving protein kinases and/or phosphatases acting directly on Ca^{++} channels" (Chiesa et al. 2000). Our study explores this hypothesis in detail and provides results supporting in part this possible explanation.

We evaluated the reduction of phosphate activity on P-ERK mediated by the PP1 since recent findings demonstrated a direct ATM-dependent activation of PP1 (Guo et al. 2007). It has been demonstrated that endogenous PP1 catalytic subunits (PP1C) strongly coimmunoprecipitates with ERK1/2 when stimulated by IGF1 treatment. Since IGF-1/IGF1R levels are downregulated in skeletal muscle of $ATM^{+/-}$ mouse (Ching et al. 2013), probably weaker interactions between PP1 and ERK1/2 occur, thus resulting in higher levels of P-ERK. Finally, we cannot exclude also a direct contribution of PP1 to the GABAergic system since it has been demonstrated that it controls GABA receptor clusterization by regulating gephyrin dephosphorylation state (Bausen et al. 2010).

Previous studies demonstrated at hippocampal synapses a link between enhanced ERK1/2 phosphorylation, higher GABAergic release, and altered learning/neuronal functioning (Cui et al. 2008). Also, increased ERK1/2 activation has been demonstrated to occur via activation of the transcription factor Egr1, which belongs to the Egr-transcription factor family (Luo et al. 2008), thus supporting the hypothesis that the increased ERK phosphorylation found in ATM-deficient cells can affect the GABAergic development and synaptogenesis.

Overall, our data demonstrating a new function of ATM in neurons individuate a possible target for the pharmacological treatment of cognitive disabilities associated with mild forms of A-T. Although further investigations need to be carried out to better individuate the precise molecular interactors involved in this process and the best pharmacological cocktail to rescue the

pathological phenotype, this study unveils an unexpected role of ATM as a protein kinase responsible, possibly through regulation of P-ERK signaling, for the correct development of the inhibitory network and maintenance of neuronal transmission.

Experimental Procedures

Animals

All the experimental procedures followed the guidelines established by the Italian Council on Animal Care and were approved by the Italian Government decree No. 27/2010 (see Supplementary Material) and the Italian Legislation (L.D. no 26/2014). All efforts were made to minimize the number of animals used and their sufferings.

Cell Cultures

Hippocampal neurons were established from E20 to P0 het or wt littermate C57BL/6 mice as described previously (Menna et al. 2009). For siRNA experiments, rat primary hippocampal neurons have been used starting from E18 pregnant animals.

Genotyping

Genotyping of ATM was performed on extracted tail DNA using polymerase chain reaction techniques. After genomic extraction, carried out using the Laird protocol (Laird et al. 1991), 3 μL final volumes of DNA were mixed in 7 μL of master mix (GoTAq Promega), 0.75 μL of oligonucleotides, and 3.75 μL of MilliQ water. The DNA was amplified using a thermo cycler (Biorad, Hercules, CA, USA).

Cell Culture Electrophysiology

Whole-cell, patch-clamp recordings were obtained from 13 to 14 DIV neurons with an Axopatch 200B amplifier and the pClamp-10 software (Axon Instruments, Foster City, CA, USA). Recordings were performed in the voltage-clamp mode. Currents were sampled at 2 kHz and filtered at 2–5 kHz. External solution [Krebs'–Ringer's–HEPES (KRH)] had the following composition (in mM): 125 NaCl, 5 KCl, 1.2 $MgSO_4$, 1.2 KH_2PO_4, 2 $CaCl_2$, 6 glucose, and 25 HEPES–NaOH, pH 7.4. mEPSCs and mIPSCs were recorded in the presence of 1 μM TTX. Recording pipettes were fabricated from capillary glass (World Precision Instruments) using a two-stage puller (Narishige, Tokyo, Japan) and had tip resistances of 3–5 M when filled with the intracellular solution of the following composition (in mM): 130 K-gluconate (or Cs-gluconate for IPSCs and mEPSCs), 10 KCl, 1 EGTA, 10 HEPES, 2 $MgCl_2$, 4 MgATP, and 0.3 Tris-GTP. Neurons were held at −70 or + 10 mV to identify, respectively, excitatory or inhibitory miniature events. Recordings were performed at room temperature. Bicuculline (5 μM) had been added in the medium of 7 and 10 DIV primary neuronal cultures and recordings performed 3 days later the last drug delivery. Offline analyses of mEPSCs and mIPSCs have been performed using Clampfit- pClamp-10 software and events had to exceed a threshold of 2 times the SD of the baseline noise.

Immunocytochemical Staining

Immunofluorescence staining was carried out using the following antibodies: mouse anti-VAMP (1 : 500), guinea pig anti-vGAT (1 : 500), rabbit anti-vGLUT1 (1 : 500), and rabbit anti-β-tubulin (1 : 80), all of them from Synaptic System. Secondary antibodies were conjugated with Alexa-488, Alexa-555, or Alexa-633 fluorophores (Invitrogen, San Diego, CA, USA). Images were acquired using an Leica SPE confocal microscope with ×60 objective. For the analysis of v-GAT density per μm of dendrite stack, images have been acquired and the Z-projection maximal mean intensity values have been obtained. The number of vGAT-positive puncta has been counted after the detection of an appropriate threshold which was set to 2.5-fold the level of background fluorescence referring to diffuse fluorescence within dendritic shafts. Fluorescence image processing and analyses were performed with ImageJ Software (National Institutes of Health). For the analysis, vGAT- and vGlut-1-positive puncta per unit length of isolated parent dendrite have been chosen by positive tubulin immunoreactivity. Field per field, isolated dendritic branches have been analyzed in segments of about 30 μm and in total, 250 dendritic segments have been analyzed in wt cultures and 300 in het cultured neurons. We estimated a number of 100 cells counted per genotyping for both vGAT and VGlut-1 puncta density.

Western Blotting

Homogenates from mouse hippocampal tissues (both P13–14 and P40 female + male animals) were separated by electrophoresis, blotted on nitrocellulose membrane, and analyzed by western blotting by using: monoclonal antibodies against ATM (1 : 350, Santa Crutz), rabbit anti-calnexin (1 : 2000, Sigma, as an internal standard for protein quantification), mouse anti-β3-tubulin (1 : 4000, Promega), rabbit anti-vGAT (1 : 1000, Synaptic System), rabbit anti-KCC2 (1 : 700, Millipore), mouse anti-P-ERK (1 : 1000, Sigma), rabbit anti-ERKtot (1 : 1000, Cell Signaling), rabbit anti-calcineurin A (1 : 1000, Cell Signaling), rabbit anti-PP1 (1 : 1000, Cell Signaling), and rabbit anti-calpain (1 : 1000, Cell Signaling). Membranes were washed and reacted with HRP-conjugated secondary antibodies (Jackson Laboratories) and developed by ECL (Amersham, UK), or reacted with fluorophor-conjugated secondary antibodies (LI-COR Biosciences™ IRDye 800CW and IRDye 680RD™, 1 : 10 000). The corresponding fluorescence signal has been acquired with CLx Odyssey (LI-COR Biosciences) and quantified using Odyssey IR Technology by the software Image Studio 2.0.

Measurements regarding the chemoluminescence have been carried out using ImageJ software 1.46r.

Calcium Imaging

Hippocampal cultures of 5–6 DIV were loaded with 5 μM Fura-2 pentacetoxymethylester in KRH for 30 min at 37 °C, washed in the same solution, and transferred to the recording chamber of an inverted microscope (Axiovert 100; Zeiss, Oberkochen, Germany) equipped with a calcium imaging unit. After a period for baseline acquisition, neurons were stimulated with GABA 100 μM and responses have been recorded. Fura-2 fluorescence images were analyzed with TILLvision software (TILL Photonics). After excitation at 340 and 380 nm wavelengths, emitted light was acquired at 505 nm at a rate of 1–4 Hz. Temporal Ca^{++} intensity profiles (expressed as F340/380 fluorescence ratio) were calculated in discrete areas of interest from image sequences. "Ratio changes" indicate the amplitude of peak Ca^{++} responses, thus indicating the depolarizing GABA action.

Acute Downregulation of ATM Expression

Silencing of ATM was achieved via transfection of siRNA duplexes against mouse Atm to achieve controlled ATM downregulation in rat primary hippocampal neurons. The siRNA was from Integrated DNA Technologies and the Atm sense strand was 50-GGAGCAUGCUCUAAGGACATT-30. Primary cultures of rat embryonic neurons were transfected with siRNA plus Lipofectamine 2000, in a first set of experiments at 8–9 DIV and in a second set of experiments at 2 DIV (in Ca^{++} imaging experiments).

Samples were mainly collected in both experimental procedures after 4–5 days.

Brain Slice and Electrophysiology

$ATM^{+/+}$ and $ATM^{+/-}$ male mice were anesthetized in a chamber saturated with chloroform and then decapitated. The brain was rapidly removed and placed in an ice-cold solution containing 220 mM sucrose, 2 mM KCl, 1.3 mM NaH_2PO_4, 12 mM $MgSO_4$, 0.2 mM $CaCl_2$, 10 mM glucose, 2.6 mM $NaHCO_3$ (pH 7.3, equilibrated with 95% O_2 and 5% CO_2), and 3 mM kynurenic acid. Coronal hippocampal slices (thickness, 300 μm) were prepared with a vibratome VT1000 S (Leica) and then incubated first for 40 min at 37 °C and then for 30 min at room temperature in artificial CSF (ACSF), consisting of 126 mM NaCl, 3 mM KCl, 1.25 mM NaH_2PO_4, 1 mM $MgSO_4$, 2 mM $CaCl_2$, 10 mM glucose, and 26 mM $NaHCO_3$ (pH 7.3, equilibrated with 95% O_2 and 5% CO_2).

Slices were transferred to a recording chamber perfused with ACSF at a rate of approximately 2 mL/min and at room temperature. Whole-cell, patch-clamp electrophysiological recordings were performed with a Multiclamp 700B amplifier (Axon CNS Molecular Devices, USA) and using an infrared-differential interference contrast microscope. Patch microelectrodes (borosilicate capillaries with a filament and an outer diameter of 1.5 μm; Sutter Instruments) were prepared with a four-step horizontal puller (Sutter Instruments) and had a resistance of 3–5 MΩ.

mIPSCs and mEPSCs were recorded from CA1 pyramidal neurons in voltage-clamp mode at a holding potential of −65 mV with an internal solution containing (in mM) 140 CsCl, 2 $MgCl_2$, 1 $CaCl_2$, 10 EGTA, 10 HEPES–CsOH, 2 ATP (disodium salt) or 126 K-gluconate, 4 NaCl, 1 EGTA, 1 $MgSO_4$, 0.5 $CaCl_2$, 3 ATP (magnesium salt), 0.1 GTP (sodium salt), 10 glucose, and 10 HEPES–KOH (pH 7.28; osmolarity adjusted to 280 mOsm), respectively. Access resistance was between 10 and 20 MΩ; if it is changed by >20% during the recording, the recording was discarded.

All the currents were recorded in the presence of lidocaine (500 μM) to block voltage-gated sodium channels in the ACSF and to prevent AP firing.

mIPSCs were recorded in the presence of kynurenic acid (3 mM) to block excitatory transmission, whereas mEPSCs were recorded in the presence of bicuculline (20 μM) to block GABAergic component.

Current-clamp analysis was performed with the same internal solution used for mEPSC recordings. A series of current steps (from −60 to 300 pA) were injected to induce APs (20-pA injection current per step, duration of 1 s) in order to study passive and active properties of the cell membrane.

Currents through the patch-clamp amplifier were filtered at 2 kHz and digitized at 20 kHz using the Clampex 10.1 software. Analysis was performed offline with the Clampfit 10.1 software.

Reagents

TTX and bicuculline were from Tocris. Cs-gluconate, CsCl, $MgSO_4$, NaCl, KH_2PO_4, K-gluconate, EGTA, HEPES, MgATP, and Tris-GTP were from Sigma-Aldrich.

Statistical Analysis

Unless otherwise stated, average data are expressed as mean ± SEM. Data were analyzed by paired/unpaired Student's *t*-test or, in case of more than 2 experimental groups, by one-way analysis of variance followed by post hoc multiple comparison tests using Sigma Stat software. Data were expressed as means ± SEM for the number of cells (n). The differences were considered to be significant, if $P < 0.05$ (indicated by an asterisk), $P < 0.01$ (double asterisks), $P < 0.005$ (triple asterisks).

Authors' Contributions

L.P. performed experiments and analyzed data. E.F. and L.M. performed experiments (biochemistry and in vivo electrophysiology, respectively) and analyzed data. M.T. provided $ATM^{-/-}$ mice and helped with some experiments. M.P. read the paper. E.M. read the paper and discussed data. M.M. discussed data and wrote the paper. F.A. designed experiments, discussed data, and wrote the paper.

Supplementary Material

Supplementary material can be found at http://www.cercor.oxfordjournals.org/.

Funding

This research has been supported by Fondo per gli Investimenti della Ricerca di Base (FIRB)-RBFR10ZBYZ to F.A. and Progetti di ricerca di Rilevante Interesse Nazionale (PRIN) 2010–2011 2010JFYFY2_008 to M.M. F.A. is supported by the Italian Ministry of Research and Education program "FIRB giovani" 2010, protocol number: RBFR10ZBYZ. M.T. is supported by Fondazione "Giancarla Vollaro", Via Filodrammatici 10, Milano. This research has been also supported by Cariplo 2012-0560 (E.M.).

Notes

Conflict of Interest: None declared.

References

Akerman CJ, Cline HT. 2007. Refining the roles of GABAergic signaling during neural circuit formation. Trends Neurosci. 30:382–389.

Allen DR, van Praag H, Ray J, Weaver Z, Winrow CJ, Carter TA, Braquet R, Harrington E, Ried T, Brown KD, et al. 2001. Ataxia telangiectasia mutated is essential during adult neurogenesis. Genes Dev. 15:554–566.

Aloj G, Giardino G, Valentino L, Maio F, Gallo V, Esposito T, Naddei R, Cirillo E, Pignata C. 2012. Severe combined immunodeficiences: new and old scenarios. Int Rev Immunol. 31:43–65.

Antonucci F, Alpar A, Kacza J, Caleo M, Verderio C, Giani A, Martens H, Chaudhry FA, Allegra M, Grosche J, et al. 2012. Cracking down on inhibition: selective removal of GABAergic interneurons from hippocampal networks. J Neurosci. 32:1989–2001.

Bausen M, Weltzien F, Betz H, O'Sullivan GA. 2010. Regulation of postsynaptic gephyrin cluster size by protein phosphatase 1. Mol Cell Neurosci. 44:201–209.

Ben-Ari Y. 2002. Excitatory actions of GABA during development: the nature of the nurture. Nat Rev Neurosci. 3:728–739.

Ben-Ari Y, Cherubini E, Corradetti R, Gaiarsa JL. 1989. Giant synaptic potentials in immature rat CA3 hippocampal neurones. J Physiol. 416:303–325.

Borghesani PR, Alt FW, Bottaro A, Davidson L, Aksoy S, Rathbun GA, Roberts TM, Swat W, Segal RA, Gu Y. 2000. Abnormal development of Purkinje cells and lymphocytes in Atm mutant mice. Proc Natl Acad Sci USA. 97:3336–3341.

Chamma I, Heubl M, Chevy Q, Renner M, Moutkine I, Eugene E, Poncer JC, Levi S. 2013. Activity-dependent regulation of the

K/Cl transporter KCC2 membrane diffusion, clustering, and function in hippocampal neurons. J Neurosci. 33:15488–15503.
Cherubini E, Gaiarsa JL, Benari Y. 1991. GABA—an excitatory transmitter in early postnatal life. Trends Neurosci. 14:515–519.
Chiesa N, Barlow C, Wynshaw-Boris A, Strata P, Tempia F. 2000. Atm-deficient mice Purkinje cells show age-dependent defects in calcium spike bursts and calcium currents. Neuroscience. 96:575–583.
Ching JK, Luebbert SH, Collins RL, Zhang ZH, Marupudi N, Banerjee S, Hurd RD, Ralston L, Fisher JS. 2013. Ataxia telangiectasia mutated impacts insulin-like growth factor 1 signalling in skeletal muscle. Exp Physiol. 98:526–535.
Chudotvorova I, Ivanov A, Rama S, Hubner CA, Pellegrino C, Ben-Ari Y, Medina I. 2005. Early expression of KCC2 in rat hippocampal cultures augments expression of functional GABA synapses. J Physiol Lond. 566:671–679.
Chun HH, Gatti RA. 2004. Ataxia-telangiectasia, an evolving phenotype. DNA Repair. 3:1187–1196.
Cui Y, Costa RM, Murphy GG, Elgersma Y, Zhu Y, Gutmann DH, Parada LF, Mody I, Silva AJ. 2008. Neurofibromin regulation of ERK signaling modulates GABA release and learning. Cell. 135:549–560.
Deidda G, Parrini M, Naskar S, Bozarth IF, Contestabile A, Cancedda L. 2015. Reversing excitatory GABAAR signaling restores synaptic plasticity and memory in a mouse model of Down syndrome. Nat Med. 21:318–326.
Di Cristo G. 2007. Development of cortical GABAergic circuits and its implications for neurodevelopmental disorders. Clin Genet. 72:1–8.
Gogolla N, Leblanc JJ, Quast KB, Sudhof TC, Fagiolini M, Hensch TK. 2009. Common circuit defect of excitatory-inhibitory balance in mouse models of autism. J Neurodev Disord. 1:172–181.
Grumelli C, Berghuis P, Pozzi D, Caleo M, Antonucci F, Bonanno G, Carmignoto G, Dobszay MB, Harkany T, Matteoli M, et al. 2008. Calpain activity contributes to the control of SNAP-25 levels in neurons. Mol Cell Neurosci. 39:314–323.
Guo C, Mi J, Brautigan DL, Larner JM. 2007. ATM regulates ionizing radiation-induced disruption of HDAC1 : PP1 : Rb complexes. Cell Signal. 19:504–510.
Harauzov A, Spolidoro M, DiCristo G, De Pasquale R, Cancedda L, Pizzorusso T, Viegi A, Berardi N, Maffei L. 2010. Reducing intracortical inhibition in the adult visual cortex promotes ocular dominance plasticity. J Neurosci. 30:361–371.
He S, Ma J, Liu N, Yu X. 2010. Early enriched environment promotes neonatal GABAergic neurotransmission and accelerates synapse maturation. J Neurosci. 30:7910–7916.
Hensch TK. 2005. Critical period plasticity in local cortical circuits. Nat Rev Neurosci. 6:877–888.
Hensch TK, Fagiolini M. 2005. Excitatory-inhibitory balance and critical period plasticity in developing visual cortex. Progr Brain Res. 147:115–124.
Herrup K, Li JL, Chen JM. 2013. The role of ATM and DNA damage in neurons: upstream and downstream connections. DNA Repair. 12:600–604.
Khanna KK, Jackson SP. 2001. DNA double-strand breaks: signaling, repair and the cancer connection. Nat Genet. 27:247–254.
Khazipov R, Esclapez M, Caillard O, Bernard C, Khalilov I, Tyzio R, Hirsch J, Dzhala V, Berger B, Ben-Ari Y. 2001. Early development of neuronal activity in the primate hippocampus in utero. J Neurosci. 21:9770–9781.
Laird PW, Zijderveld A, Linders K, Rudnicki MA, Jaenisch R, Berns A. 1991. Simplified mammalian DNA isolation procedure. Nucleic Acids Res. 19:4293.
Lee JH, Kim KH, Morio T, Kim H. 2006. Ataxia-telangiectasia-mutated-dependent activation of Ku in human fibroblasts exposed to hydrogen peroxide. Ann N Y Acad Sci. 1091:76–82.
Li JL, Han YR, Plummer MR, Herrup K. 2009. Cytoplasmic ATM in neurons modulates synaptic function. Curr Biol. 19:2091–2096.
Lim DS, Kirsch DG, Canman CE, Ahn JH, Ziv Y, Newman LS, Darnell RB, Shiloh Y, Kastan MB. 1998. ATM binds to beta-adaptin in cytoplasmic vesicles. Proc Natl Acad Sci USA. 95:10146–10151.
Lu J, Karadsheh M, Delpire E. 1999. Developmental regulation of the neuronal-specific isoform of K-Cl cotransporter KCC2 in postnatal rat brains. J Neurobiol. 39:558–568.
Ludwig A, Uvarov P, Soni S, Thomas-Crusells J, Airaksinen MS, Rivera C. 2011. Early growth response 4 mediates BDNF induction of potassium chloride cotransporter 2 transcription. J Neurosci. 31:644–649.
Luo Y, Lathia J, Mughal M, Mattson MP. 2008. SDF1alpha/CXCR4 signaling, via ERKs and the transcription factor Egr1, induces expression of a 67-kDa form of glutamic acid decarboxylase in embryonic hippocampal neurons. J Biol Chem. 283:24789–24800.
Maya-Vetencourt JF, Baroncelli L, Viegi A, Tiraboschi E, Castren E, Cattaneo A, Maffei L. 2012. IGF-1 restores visual cortex plasticity in adult life by reducing local GABA levels. Neural Plast. 2012:631965.
Menna E, Disanza A, Cagnoli C, Schenk U, Gelsomino G, Frittoli E, Hertzog M, Offenhauser N, Sawallisch C, Kreienkamp HJ, et al. 2009. Eps8 regulates axonal filopodia in hippocampal neurons in response to brain-derived neurotrophic factor (BDNF). PLoS Biol. 7:e1000138.
Nakayama H, Miyazaki T, Kitamura K, Hashimoto K, Yanagawa Y, Obata K, Sakimura K, Watanabe M, Kano M. 2012. GABAergic inhibition regulates developmental synapse elimination in the cerebellum. Neuron. 74:384–396.
Owens DF, Kriegstein AR. 2002. Is there more to GABA than synaptic inhibition? Nat Rev Neurosci. 3:715–727.
Rivera C, Voipio J, Payne JA, Ruusuvuori E, Lahtinen H, Lamsa K, Pirvola U, Saarma M, Kaila K. 1999. The K^+/Cl^- co-transporter KCC2 renders GABA hyperpolarizing during neuronal maturation. Nature. 397:251–255.
Sale A, Berardi N, Spolidoro M, Baroncelli L, Maffei L. 2010. GABAergic inhibition in visual cortical plasticity. Front Cell Neurosci. 4:10.
Shiloh Y. 2006. The ATM-mediated DNA-damage response: taking shape. Trends Biochem Sci. 31:402–410.
Succol F, Fiumelli H, Benfenati F, Cancedda L, Barberis A. 2012. Intracellular chloride concentration influences the GABA(A) receptor subunit composition. Nat Commun. 3:738.
Sun C, Zhang L, Chen G. 2013. An unexpected role of neuroligin-2 in regulating KCC2 and GABA functional switch. Mol Brain. 6:23.
Tyzio R, Cossart R, Khalilov I, Minlebaev M, Hubner CA, Represa A, Ben-Ari Y, Khazipov R. 2006. Maternal oxytocin triggers a transient inhibitory switch in GABA signaling in the fetal brain during delivery. Science. 314:1788–1792.
Tyzio R, Nardou R, Ferrari DC, Tsintsadze T, Shahrokhi A, Eftekhari S, Khalilov I, Tsintsadze V, Brouchoud C, Chazal G, et al. 2014. Oxytocin-mediated GABA inhibition during delivery attenuates autism pathogenesis in rodent offspring. Science. 343:675–679.
van den Pol AN, Obrietan K, Chen G. 1996. Excitatory actions of GABA after neuronal trauma. J Neurosci. 16:4283–4292.
Volkow ND, Tomasi D, Wang GJ, Studentsova Y, Margus B, Crawford TO. 2014. Brain glucose metabolism in adults with ataxia-telangiectasia and their asymptomatic relatives. Brain. 137:1753–1761.